Planar path following of underwater snake robots in the presence of ocean currents

A. M. Kohl[1], K. Y. Pettersen[1], E. Kelasidi[1], and J. T. Gravdahl[2]

***Abstract*—This paper presents a control system that enables an underwater snake robot to converge towards and follow a straight path in the presence of constant irrotational ocean currents. The robot is assumed to be neutrally buoyant, fully submerged and moving in a virtual plane with a sinusoidal gait and limited link angles. The proposed control approach uses a heading controller that exponentially stabilises the heading of the robot towards the desired heading, which is obtained by an integral line-of-sight guidance law. Uniform semi-global exponential stability of the control system is formally proved using cascaded systems and Lyapunov theory. Simulations are presented that illustrate and validate the theoretical results.**

***Index Terms*—Biologically-Inspired Robots; Marine Robotics; Underactuated Robots**

I. Introduction

In underwater operations, a higher level of autonomy is desired. Amphibious and underwater snake robots (USRs) are considered promising to improve the autonomy, efficiency, and maneuverability of next generation underwater vehicles, and have therefore experienced a lot of research interest recently. In order to realise operational snake robots for such underwater applications, a number of different control design challenges must be solved. One important problem concerns the ability of such robots to follow a desired path, which will be addressed in this paper.

The mathematical modelling of USRs or eel-like robots [1–4], as well as the development of prototypes [5–7] have been given increasing attention lately. Even more recently, the development of path planning and guidance algorithms for such robots are moving into focus. In [8], the authors propose a virtual-target guidance law for path-following of an eel-like robot. In [9], a line-of-sight (LOS) guidance law for a 3-linked robot fish is developed. However, neither [8] nor [9] consider currents, nor are the proposed methods formally proved. For ground snake robots, a LOS guidance law has been proved to κ-exponentially stabilise the robot to a straight path in [10,11]. This work was extended to include velocity control in [12]. For USRs, however, the same method cannot guarantee path-following, because disturbances by ocean currents are not considered. A method that is often used for the guidance of marine vessels [13–16] and AUVs [17] and which handles the problem of ocean current disturbances causing drift, is integral line-of-sight (ILOS) guidance. For this method, integral action is added to the traditional LOS guidance law. Based on the stability analysis of LOS guidance in [18], ILOS guidance was shown to be uniformly semi-globally exponentially stable (USGES) for surface vessels in [16]. A first step towards applying ILOS also to USRs exposed to currents has been made in [19] based on a complex model of underwater snake robots. There, a simple P-controller is used to steer the robot towards the desired heading that is obtained with an ILOS guidance law. Stability is shown for certain numerical values with a Poincaré map. However, to the authors' best knowledge, no general formal stability proof for path-following of USRs exposed to currents has been presented yet.

The first contribution of this paper is the development of a control system that enables a USR to converge to and follow a straight path in a virtual plane in the presence of constant irrotational currents. A heading controller is designed that exponentially stabilises the heading of the robot towards the heading given by an ILOS guidance law. Unlike previous approaches for ground robots [10,11], this control system is able to handle the disturbance produced by the ocean current. The second and main contribution of this paper compared to previous work [19] is the stability analysis. Using cascaded systems theory, it is formally proved that under the assumption of positive forward velocity, the cross-track error between the robot and the desired path is both uniformly globally asymptotically stable (UGAS) and USGES. The control system is thus guaranteed to fulfil the control objective.

The paper is organised as follows: In Sec. II, a stability definition and the non-linear cascaded systems theory that is required are shortly summarized. Sec. III briefly presents a model of a USR that has previously been developed in [20,21], and will serve as the basis for the control system in this paper. The control system and the stability analysis of the closed-loop system are presented in Sec. IV. Simulation results are presented in Sec. V. Conclusions and suggestions for further work are given in Sec. VI.

II. Mathematical preliminaries

This sections briefly recalls the definition of exponential stability and two stability theorems that will serve as the basis for proving stability of the path following control system in

Manuscript received: August, 31, 2015; Revised November, 12, 2015; Accepted December, 28, 2015.

This paper was recommended for publication by Editor Yu Sun upon evaluation of the Associate Editor and Reviewers' comments. This work was partly supported by the Research Council of Norway through its Centres of Excellence funding scheme, project no. 223254-AMOS.

[1]A. M. Kohl, K. Y. Pettersen, and E. Kelasidi are with the Centre for Autonomous Marine Operations and Systems (AMOS), Department of Engineering Cybernetics at NTNU, NO-7491 Trondheim, Norway Anna.Kohl@itk.ntnu.no

[2]J. T. Gravdahl is with the Department of Engineering Cybernetics at NTNU, Norway Tommy.Gravdahl@itk.ntnu.no

Digital Object Identifier (DOI): see top of this page.

Sec. IV. For simplicity, we often say that a system is stable, if the equilibrium $x = 0$ of the system is stable.

Definition 1 (see Definition 2.7 in [22]): The origin of a system $\dot{x} = f(t, x)$ is said to be uniformly locally exponentially stable (ULES) if there exist constants $\gamma_1, \gamma_2, r > 0$ such that for all $(t_0, x(t_0)) \in \mathbb{R}_{\geq 0} \times \mathcal{B}_r$

$$\|x(t, t_0, x(t_0))\| \leq \gamma_1 \|x(t_0)\| e^{-\gamma_2 (t - t_0)} \quad \forall t \geq t_0. \tag{1}$$

If for each $r > 0$ there exist γ_1, γ_2 such that (1) holds for all $(t_0, x(t_0)) \in \mathbb{R}_{\geq 0} \times \mathcal{B}_r$ then, the system is said to be uniformly semi-globally exponentially stable (USGES).

The system that will be studied is a cascaded nonlinear time-varying system of the structure that was defined in [23]:

$$\begin{aligned} \Sigma_1 : \ \dot{x}_1 &= f_1(t, x_1) + g(t, x) x_2, \\ \Sigma_2 : \ \dot{x}_2 &= f_2(t, x_2) \end{aligned} \tag{2}$$

For the stability analysis of such systems, the following theory can be applied.

Theorem 1 (see Theorem 2 in [23]): If the following assumptions are satisfied, the cascaded system (2) is UGAS.

1) $\dot{x}_1 = f_1(x_1, t)$ is UGAS with a radially unbounded Lyapunov function satisfying

$$\begin{aligned} \|\frac{\partial V}{\partial x_1}\| \|x_1\| \leq c_1 V(t, x_1) \quad & \forall \|x_1\| \geq \eta, \\ \|\frac{\partial V}{\partial x_1}\| \leq c_2, \quad & \forall \|x_1\| \leq \eta, \end{aligned} \tag{3}$$

   with $c_1, c_2, \eta > 0$.
2) $\|g(t, x))\| \leq \theta_1(\|x_2\|) + \theta_2(\|x_2\|)\|x_1\|$, where $\theta_1, \theta_2 : \mathbb{R}_{\geq 0} \mapsto \mathbb{R}_{\geq 0}$ cont.,
3) Σ_2 is UGAS and

$$\int_{t_0}^{\infty} \|x_2(t)\| \mathrm{d}t \leq \phi(\|x_2(t_0)\|), \tag{4}$$

   $\phi(\cdot)$ is a class $\mathcal{K}$ function.

In particular, Ass. 1) always holds for a quadratic Lyapunov function V [23], and Ass. 3) is always fulfilled if Σ_2 is κ-exponentially stable [11], i.e. UGAS and ULES [24].

Proposition 1 (see Prop. 2.3 in [22]): If in addition to the assumptions in Th. 1 the systems Σ_2 and $\dot{x}_1 = f_1(x_1, t)$ are USGES then the cascaded system (2) is USGES and UGAS. If the subsystems are UGES the cascade is UGES.

III. The Model of the USR

This section introduces the control-oriented model of a USR that will be used as a basis for the control system.

A. Overview of the model

The control-oriented model is aimed at the design and analysis of motion planning and control systems of a USR in slow transit mode. It was derived from a complex model which was presented in [1]. The complex model considers the full kinematics and dynamics of a planar snake robot with revolute joints and is based on the Newton-Euler formulation. It takes into account both linear and nonlinear drag forces, added mass effects and a constant ocean current. Despite the complexity, the equations of motion are presented in closed form. However, the model in [1] is still too complex for the design of motion planning and control systems. In [25], a first step was taken towards the control-oriented modelling of USRs for the special case of no current, based on a simplified approach that was suggested for ground snake robots in [26].

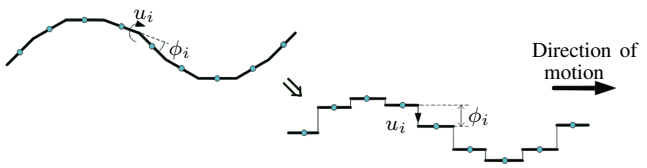

Fig. 1. Modelling of the revolute joints as prismatic joints [26]

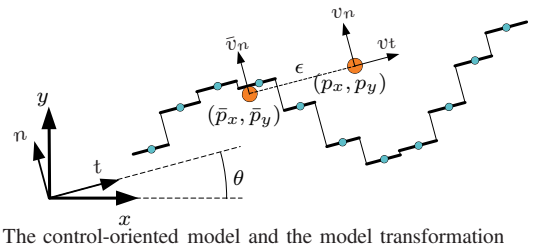

Fig. 2. The control-oriented model and the model transformation

Later, a control-oriented model of a USR exposed to currents was presented in [20]. The assumptions on which the control-oriented model is based are:

- The drag coefficient in normal direction is larger than in tangential direction.
- The USR is moving slowly with the gait lateral undulation and limited link angles.

The complex model from [1] was analysed under these assumptions. It turned out that the rotational motion of each link in essence results in a translational displacement of each link, and that it is this displacement that propels the USR. Based on these observations, the key assumption for the control-oriented model is that the overall behaviour of the USR can be captured by looking at the link translation relative to the direction of motion, as visualised in Fig. 1. The control-oriented model was further simplified and extended to arbitrary sinusoidal gaits in [21]. There, the model is validated by an extensive simulation study, which compares the behaviour of the control-oriented model with the first-principle model from [1]. In addition, the control-oriented model without currents was validated experimentally [27].

B. Equations of motion

The USR is assumed to consist of N links of length $L = 2l$ and mass m, that are connected by $N - 1$ joints. The robot thus has $N + 2$ degrees of freedom, two corresponding to the position in the plane (p_x, p_y), $N-1$ corresponding to the joint coordinates ϕ_i, and one to the orientation θ. For the description of the USR, two coordinate frames are introduced: the global x-y-frame, and the body-aligned t-n-frame. With a linearising feedback law, the joint coordinates ϕ_i are directly controlled by the input $\bar{\mathbf{u}} \in \mathbb{R}^{N-1}$, details on the controller can be found in [21]. The geometry and different coordinate frames of the model can be seen in Fig. 2. The dynamical equations, on which the development of the path following controller will be based are:

$$\dot{\boldsymbol{\phi}} = \mathbf{v}_{\phi}, \tag{5a}$$

$$\dot{\theta} = v_\theta, \tag{5b}$$
$$\dot{p}_x = v_t \cos\theta - v_n \sin\theta, \tag{5c}$$
$$\dot{p}_y = v_t \sin\theta + v_n \cos\theta, \tag{5d}$$
$$\dot{\mathbf{v}}_\phi = \bar{\mathbf{u}}, \tag{5e}$$
$$\dot{v}_\theta = -\lambda_1 v_\theta + \tfrac{\lambda_2}{N-1} v_{t,\mathrm{rel}} \bar{\mathbf{e}}^T \boldsymbol{\phi}, \tag{5f}$$
$$\dot{v}_t = -\tfrac{c_t}{m} v_{t,\mathrm{rel}} + \tfrac{2c_p}{Nm} \bar{\mathbf{e}}^T \boldsymbol{\phi} v_{n,\mathrm{rel}} - \tfrac{c_p}{Nm} \boldsymbol{\phi}^T \mathbf{A} \bar{\mathbf{D}} \mathbf{v}_\phi, \tag{5g}$$
$$\dot{v}_n = \tfrac{2c_p}{Nm} \bar{\mathbf{e}}^T \boldsymbol{\phi} v_{t,\mathrm{rel}} - \tfrac{c_n}{m} v_{n,\mathrm{rel}}. \tag{5h}$$

In (5), the vector $\boldsymbol{\phi} \in \mathbb{R}^{N-1}$ contains all joint coordinates ϕ_i and the parameters λ_i are empirical constants characterising the rotational dynamics. The parameters c_n, c_t define the drag parameters in normal and tangential direction of the robot, respectively, and the parameter c_p is a propulsion coefficient. The variables $v_{n,\mathrm{rel}}, v_{t,\mathrm{rel}}$ denote the relative velocity in normal and tangential direction, respectively. The remaining vectors and matrices are the summation vector $\bar{\mathbf{e}} = \begin{bmatrix} 1 & \dots & 1 \end{bmatrix}^T \in \mathbb{R}^{N-1}$, the matrix $\bar{\mathbf{D}} = \mathbf{D}^T \left(\mathbf{D}\mathbf{D}^T\right)^{-1}$, with $\mathbf{D} = \begin{bmatrix} 1 & -1 & & \\ & \ddots & \ddots & \\ & & 1 & -1 \end{bmatrix}$, and $\mathbf{A} = \begin{bmatrix} 1 & 1 & & \\ & \ddots & \ddots & \\ & & 1 & 1 \end{bmatrix}$, $\mathbf{D}, \mathbf{A} \in \mathbb{R}^{(N-1)\times N}$. More details can be found in [20,21].

IV. The Path Following Control System

This section presents the control system that is proposed for the path-following of a USR. At first, underlying assumptions are introduced, then the model is transformed to a form that is more suitable for the control design, and the control objective is formulated. Next, the control system, consisting of an underlying gait controller and a heading controller, is presented. Finally, the stability analysis of the resulting control system is presented and proved as the main result.

A. Assumptions

For the USR, that is described by the model (5) and moving with a sinusoidal gait in a virtual plane, the following assumptions hold:

Assumption 1: The ocean current $\mathbf{v}_c = [V_x, \ V_y]^T$ is constant and irrotational in the global frame. It is furthermore bounded by $V_{c,\max} \geq \sqrt{V_x^2 + V_y^2}$.

Assumption 2: The USR is moving with a relative forward velocity $v_{t,\mathrm{rel}}(t) \in [V_{\min}, V_{\max}] \ \forall t \geq 0$ with the constant bounds $V_{\max} \geq V_{\min} > 0$.

Remark 1: Controlling the exact value of $v_{t,\mathrm{rel}}$ remains a topic of future work. However, it has been shown in [21] that for a sinusoidal gait, the average $v_{t,\mathrm{rel}}$ converges to a constant value given by the design parameters of the gait.

Assumption 3: The forward velocity is large enough to compensate for the current, i.e. $v_{t,\mathrm{rel}}(t) > V_{\min} > V_{c,\max}$.

B. Model transformation

In order to make the model (5) more suitable for control-design, a two-step model transformation is employed. In the first step the point that defines the position of the robot is moved in order to provide a simpler reference. In the second step the absolute velocities are eliminated from the model equations such that only the relative velocities are considered. These transformation steps simplify the controller design and are the basis for achieving a closed-loop system with a cascaded structure.

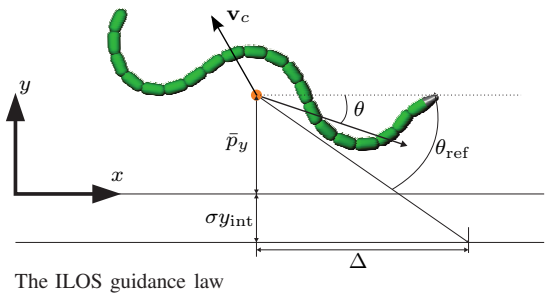

Fig. 3. The ILOS guidance law

In the dynamical equations (5f) and (5h) it can be seen that the joint coordinates $\boldsymbol{\phi}$ enter the dynamics of both v_n and v_θ. As pointed out in [11], this complicates the controller design and analysis. Motivated by [28,29], it is suggested in [11] to solve the problem by moving the point that defines the position of the snake robot by a distance ϵ in the tangential direction, from the CM to the pivot point, as can be seen in Fig. 2. The coefficient ϵ is obtained from (5f) and (5h):

$$\epsilon = -\tfrac{2(N-1)c_p}{Nm\lambda_2} \tag{6}$$

Like in [11], the new coordinates are then defined as

$$\bar{p}_x = p_x + \epsilon \cos\theta, \tag{7a}$$
$$\bar{p}_y = p_y + \epsilon \sin\theta, \tag{7b}$$
$$\bar{v}_n = v_n + \epsilon v_\theta. \tag{7c}$$

The absolute velocities are removed from (5) by inserting the relations $[v_t, \ \bar{v}_n]^T = [v_{t,\mathrm{rel}} + V_t, \ \bar{v}_{n,\mathrm{rel}} + V_n]^T$, where $V_t = V_x \cos\theta + V_y \sin\theta$, and $V_n = -V_x \sin\theta + V_y \cos\theta$ are the current velocities in the body frame, and $\dot{\bar{v}}_n = \dot{\bar{v}}_{n,\mathrm{rel}} + \dot{V}_n$, with $\dot{V}_n = -V_t \dot{\theta}$ [30].

Using the transformation (7b, 7c) and the relative velocities, the model written in the new coordinates is

$$\dot{\boldsymbol{\phi}} = \mathbf{v}_\phi, \tag{8a}$$
$$\dot{\theta} = v_\theta, \tag{8b}$$
$$\dot{\bar{p}}_y = v_{t,\mathrm{rel}} \sin\theta + \bar{v}_{n,\mathrm{rel}} \cos\theta + V_y, \tag{8c}$$
$$\dot{\mathbf{v}}_\phi = \bar{\mathbf{u}}, \tag{8d}$$
$$\dot{v}_\theta = -\lambda_1 v_\theta + \tfrac{\lambda_2}{N-1} v_{t,\mathrm{rel}} \bar{\mathbf{e}}^T \boldsymbol{\phi}, \tag{8e}$$
$$\dot{\bar{v}}_{n,\mathrm{rel}} = (X + V_t) v_\theta + Y \bar{v}_{n,\mathrm{rel}}, \tag{8f}$$

where X and Y are defined as $X = \epsilon(\tfrac{c_n}{m} - \lambda_1), Y = -\tfrac{c_n}{m}$.

Remark 2: In accordance with Ass. 2 and the procedure in [11], the relative forward velocity $v_{t,\mathrm{rel}}$ is treated as a positive parameter, whose dynamics is not controlled. Therefore, (5g) does not show up in the transformed model.

Remark 3: V_t depends on the heading angle θ. Compared to the surface vessel model from [30] with relative velocities, on which the controllers in [14,15] are based, an additional term has to be considered in the stability analysis.

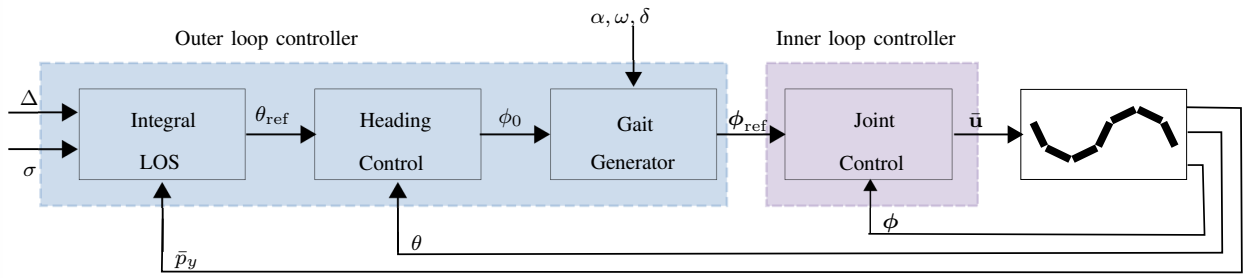

Fig. 4. The structure of the control system

C. Control objective

In this section, the control problem solved in this paper is formulated. The control system is supposed to make the USR converge to and subsequently follow a desired straight path $\mathcal{P}$ with some sufficiently large velocity $v_{t,\text{rel}} > 0$. For simplicity, the inertial coordinate frame is without loss of generality defined such that the desired path $\mathcal{P}$ is aligned with the global x-axis. The cross-track error is then defined by the USR's position $\bar{p}_y$, and the control objectives are

$$\lim_{t\to\infty} \bar{p}_y(t) = 0, \qquad (9) \qquad\qquad \lim_{t\to\infty} \theta(t) = \theta^{\text{eq}}. \qquad (10)$$

The desired heading angle θ^{eq} is constant and $\theta^{\text{eq}} \in (-\frac{\pi}{2}, \frac{\pi}{2})$. The equilibrium orientation θ^{eq} is in general non-zero [19], thus providing a side-slip angle that allows the robot to compensate for the transversal current-component, as can be seen in Fig. 3. Its value will be defined later.

D. Control system

The control law that is designed to meet the control objectives (9, 10) will be presented in the following. Motivated by [11], it consists of two components, the gait controller for propulsion, and the heading controller for the path following. The structure of the control system can be seen in Fig. 4.

1) Gait controller: As shown in [21], forward motion by a sinusoidal gait is achieved by controlling ϕ_i according to

$$\phi_{i,\text{ref}} = \alpha g(i) \sin\left(\omega t + (i-1)\delta\right) + \phi_0, \qquad (11)$$

where α is the maximum amplitude, ω is the frequency, δ is the phase shift, and ϕ_0 is a constant offset that induces turning motion. The function $g : \mathbb{R} \mapsto [0, 1]$ scales the amplitude of the single joints ϕ_i. With the control law

$$\bar{\mathbf{u}} = \ddot{\boldsymbol{\phi}}_{\text{ref}} + k_{v_\phi}(\dot{\boldsymbol{\phi}}_{\text{ref}} - \dot{\boldsymbol{\phi}}) + k_\phi(\boldsymbol{\phi}_{\text{ref}} - \boldsymbol{\phi}) \qquad (12)$$

with the scalar control gains $k_{v_\phi}, k_\phi > 0$, and (8a, 8d), the dynamics of the joint error $\widetilde{\boldsymbol{\phi}} = \boldsymbol{\phi} - \boldsymbol{\phi}_{\text{ref}}$ can be written as

$$\ddot{\widetilde{\boldsymbol{\phi}}} + k_{v_\phi}\dot{\widetilde{\boldsymbol{\phi}}} + k_\phi\widetilde{\boldsymbol{\phi}} = 0. \qquad (13)$$

2) Heading controller: The ILOS method has first been proposed for marine surface vessels in [13], where integral action was added to the traditional LOS guidance law in order to compensate for the disturbance by the current. Based on [13], the desired heading angle for the USR is defined as

$$\theta_{\text{ref}} = -\arctan\left(\tfrac{\bar{p}_y + \sigma y_{\text{int}}}{\Delta}\right), \qquad (14a)$$

$$\dot{y}_{\text{int}} = \tfrac{\Delta \bar{p}_y}{(\bar{p}_y + \sigma y_{\text{int}})^2 + \Delta^2}, \qquad (14b)$$

with the look-ahead distance $\Delta > 0$ and the integral gain $\sigma > 0$. Note that (14b) includes an anti-windup effect as $\dot{y}_{\text{int}}$ converges to zero when the cross track error $\bar{p}_y$ is large.

As proposed in [10] for ground robots, the joint-offset ϕ_0 in (11) will be used to ensure that the heading θ tracks the desired heading θ_{ref} in (14a), and the error $\widetilde{\theta} = \theta - \theta_{\text{ref}}$ thus goes to zero. Along the lines of the derivation for ground robots in [11], from expanding (8e) and inserting the relation $\boldsymbol{\phi} = \widetilde{\boldsymbol{\phi}} + \boldsymbol{\phi}_{\text{ref}}$ we see that choosing

$$\phi_0 = \tfrac{1}{\lambda_2 v_{t,\text{rel}}}\Big[\ddot{\theta}_{\text{ref}} + \lambda_1\dot{\theta}_{\text{ref}} - k_\theta(\theta - \theta_{\text{ref}}) - \tfrac{\lambda_2}{N-1} v_{t,\text{rel}} \sum_{i=1}^{N-1} \alpha g(i) \sin\left(\omega t + (i-1)\delta\right)\Big] \qquad (15)$$

yields the following error dynamics of the heading angle:

$$\ddot{\widetilde{\theta}} + \lambda_1\dot{\widetilde{\theta}} + k_\theta\widetilde{\theta} = \tfrac{\lambda_2}{N-1} v_{t,\text{rel}} \bar{\mathbf{e}}^T \widetilde{\boldsymbol{\phi}}. \qquad (16)$$

Remark 4: In (15), a singularity will occure when $v_{t,\text{rel}} = 0$. Note, however, that by Ass. 2, $v_{t,\text{rel}} > 0 \ \forall t$. By a proper choice of the gait parameters, the average forward velocity will converge to a positive value [21]. When implementing the control system, the singularity problem can be circumvented by only starting the heading controller after the USR has gained a sufficiently large forward velocity.

E. Main result

This section presents the conditions under which the control system proposed in Sec. IV-D is guaranteed to achieve the control objective formulated in Sec. IV-C.

Theorem 2: Consider a fully submerged, neutrally buoyant USR described by (8) that moves with a planar sinusoidal gait, exposed to a constant irrotational current. Suppose that Ass. 1 to 3 are fulfilled. If the look-ahead distance Δ and the integral gain σ are chosen such that

$$\Delta > \tfrac{|X| + 2V_{c,\max}}{|Y|}\left[\tfrac{5}{4}\tfrac{V_{\max} + V_{c,\max} + \sigma}{V_{\min} - V_{c,\max} - \sigma} + 1\right], \qquad (17a)$$

$$0 < \sigma < V_{\min} - V_{c,\max}, \qquad (17b)$$

then the control system described in Sec. IV-D guarantees that the control objectives (9) and (10) are achieved. Control objective (10) is met with

$$\theta^{\text{eq}} = -\arctan\left(\tfrac{V_y}{\sqrt{v_{t,\text{rel}}^2 - V_y^2}}\right). \qquad (18)$$

Proof: The proof will be given in Sec. IV-F. ■

F. Proof of the main result

The main theorem will be proved in three steps, applying cascaded systems theory that has been presented in [22,23]. For more details on the theorems that will be used in the following proof, the reader is referred to the theoretical background in [22,23].

The first step of the proof is to transform the complete system to a cascaded system. In the second step we consider the stability of the perturbing system. In the third step the stability of the nominal perturbed system will be analysed. Finally, a bound on the interconnection term will be derived, which concludes the stability proof.

The dynamics of the cross-track and the relative normal velocity are obtained from (14b), (8c) and (8f):

$$\dot{y}_{\text{int}} = \frac{\Delta \bar{p}_y}{(\bar{p}_y+\sigma y_{\text{int}})^2+\Delta^2}, \tag{19a}$$

$$\dot{\bar{p}}_y = v_{t,\text{rel}} \sin\theta + \bar{v}_{n,\text{rel}} \cos\theta + V_y, \tag{19b}$$

$$\dot{\bar{v}}_{n,\text{rel}} = (X + V_x \cos\theta + V_y \sin\theta) v_\theta + Y \bar{v}_{n,\text{rel}}. \tag{19c}$$

The equilibrium of this system is

$$y_{\text{int}}^{\text{eq}} = \frac{\Delta}{\sigma} \frac{V_y}{\sqrt{v_{t,\text{rel}}^2 - V_y^2}},\ y^{\text{eq}} = 0,\ \bar{v}_{n,\text{rel}}^{\text{eq}} = 0. \tag{20}$$

With $\theta = \theta_{\text{ref}} + \widetilde{\theta}$ and $v_\theta = \dot{\theta}_{\text{ref}} + \dot{\widetilde{\theta}}$, the relations

$$\sin\theta = \frac{\sin\widetilde{\theta}\Delta}{\sqrt{(\bar{p}_y+\sigma y_{\text{int}})^2+\Delta^2}} - \frac{\cos\widetilde{\theta}(\bar{p}_y+\sigma y_{\text{int}})}{\sqrt{(\bar{p}_y+\sigma y_{\text{int}})^2+\Delta^2}} \tag{21a}$$

$$\cos\theta = \frac{\cos\widetilde{\theta}\Delta}{\sqrt{(\bar{p}_y+\sigma y_{\text{int}})^2+\Delta^2}} + \frac{\sin\widetilde{\theta}(\bar{p}_y+\sigma y_{\text{int}})}{\sqrt{(\bar{p}_y+\sigma y_{\text{int}})^2+\Delta^2}} \tag{21b}$$

$$v_\theta = -\frac{\Delta}{(\bar{p}_y+\sigma y_{\text{int}})^2+\Delta^2}(\dot{\bar{p}}_y + \sigma \dot{y}_{\text{int}}) + \dot{\widetilde{\theta}} \tag{21c}$$

can be derived. With (21) and the new set of variables $e_1 = y_{\text{int}} - y_{\text{int}}^{\text{eq}}$, $e_2 = \bar{p}_y + \sigma e_1$, $e_3 = \bar{v}_{n,\text{rel}}$, $\boldsymbol{\eta} = [\widetilde{\boldsymbol{\phi}}^{\,T},\ \dot{\widetilde{\boldsymbol{\phi}}}^{\,T}]^T$ and $\boldsymbol{\xi} = [\widetilde{\theta},\ \dot{\widetilde{\theta}}]^T$, the whole system can be re-written as

$$[\dot{e}_1,\ \dot{e}_2,\ \dot{e}_3]^T = \mathbf{A}_e [e_1,\ e_2,\ e_3]^T + \mathbf{B} f(e_2) + \mathbf{H}_\xi \boldsymbol{\xi}, \tag{22a}$$

$$\dot{\boldsymbol{\xi}} = \begin{bmatrix} 0 & 1 \\ -k_\theta & -\lambda_1 \end{bmatrix} \boldsymbol{\xi} + \begin{bmatrix} 0_{1\times(N-1)} & 0_{1\times(N-1)} \\ \frac{\lambda_2}{N-1} v_{t,\text{rel}} \bar{\mathbf{e}}^T & 0_{1\times(N-1)} \end{bmatrix} \boldsymbol{\eta}, \tag{22b}$$

$$\dot{\boldsymbol{\eta}} = \begin{bmatrix} 0_{(N-1)\times(N-1)} & \mathbf{I}_{(N-1)} \\ -k_\phi \mathbf{I}_{(N-1)} & -k_{v_\phi} \mathbf{I}_{(N-1)} \end{bmatrix} \boldsymbol{\eta} \tag{22c}$$

where $\mathbf{H}_\xi$ contains all terms that vanish at $\boldsymbol{\xi} = 0$. The expressions for $\mathbf{A}_e, \mathbf{B},\ f(e_2), \mathbf{H}_\xi$ are given in App. A. The closed-loop system (22) is a cascaded system with (22a) as the perturbed system and (22b, 22c) as the perturbing system. Furthermore, the perturbing system (22b, 22c) is a cascaded system by itself. Note that it has the same structure like the perturbing system for ground snake robots in Chap. 8 in [11].

Lemma 1: The origin of the system (22b, 22c) is UGES.

Proof: Both system matrices in (22b), (22c) are Hurwitz, and the interconnection matrix is bounded. By Proposition 1, the perturbing system is therefore UGES. ∎

UGES is the strongest stability property and implies both UGAS, USGES and κ-exponential stability of (22b, 22c).

Remark 5: Note that the structure of (22b, 22c) is almost identical to (8.36b, 8.36c) in [11]. In [11], however, it is only explicitly concluded that the origin of the respective system is κ-exponentially stable. This suffices for the proof of global κ-exponential stability for the closed-loop system of a ground snake robot that was presented in [11]. In this paper, on the other hand, the stronger stability property UGES is shown in order to prove semi-global stability of the whole system. Since a ground robot can be considered a special case of system (22) when setting the current to zero and replacing the drag parameters by friction coefficients, the results presented in this paper are an extension to the analysis in [11].

Next we consider the unperturbed nominal system

$$[\dot{e}_1,\ \dot{e}_2,\ \dot{e}_3]^T = \mathbf{A}_e [e_1,\ e_2,\ e_3]^T + \mathbf{B} f(e_2), \tag{23}$$

where $(\boldsymbol{\eta}, \boldsymbol{\xi}) = 0$. The structure of (23) is similar to the one of the nominal system in [15].

Lemma 2: The nominal system (23) is USGES with a quadratic Lyapunov function candidate $V = \frac{1}{2}\sigma^2 e_1^2 + \frac{1}{2} e_2^2 + \frac{1}{2}\mu e_3^2,\ \mu > 0$.

Proof: The proof is given in App. B. ∎

According to Th. 1, the cascaded system (22) is UGAS, when Lemmata 1 and 2 hold and the interconnection term $\mathbf{H}_\xi$ is bounded by $\|\mathbf{H}_\xi\| \leq \mathcal{F}_1(\boldsymbol{\xi}) + \mathcal{F}_2(\boldsymbol{\xi})\|\boldsymbol{e}\|$.

Lemma 3: The induced 2-norm of the interconnecting matrix $\mathbf{H}_\xi$ in (22a) is trivially bounded by $\|\mathbf{H}_\xi\|_2 \leq \mathcal{F}_1 + \mathcal{F}_2\|\boldsymbol{e}\|_2$, where $\mathcal{F}_1$ and $\mathcal{F}_2$ are strictly positive constants.

Proof: The proof is given in App. C. ∎

With these three lemmata we can now conclude that the complete system (22) is UGAS. Since both nominal systems are in addition USGES, the system (22) is by Proposition 1 also USGES. Hence, the control objectives are achieved with θ^{eq} defined in (18). ∎

Remark 6: Note that the exponential stability property of the control system provides some robustness to disturbances and modelling errors, cf. Lemmata 9.1-9.2 in [31].

V. Case Study

This section presents simulation results that demonstrate the performance of the control system proposed in Sec. IV.

A. Simulation set-up

The model of the USR and the path-following control system were implemented and simulated in Matlab R2014b. The dynamics was computed using the *ode45* solver with both the relative and absolute error tolerance set to 10^{-4}.

A USR with $N = 10$ links was considered. The simulation parameters were chosen in accordance with the parameters of the physical snake robot Mamba [32]. In particular, the length of each link was $L = 18$ cm, the drag parameters $c_n = 17.3, c_t = 4.45$, and the propulsion coefficient $c_p = 35.69$. The rotation parameters were $\lambda_1 = 6, \lambda_2 = 120$. The mass of each link was assumed to be $m = 1.56$ kg in order to fulfil the assumption of neutral buoyancy. From these values, the distance ϵ was computed by (6) as $\epsilon = -34.3$ cm. The robot was exposed to a constant irrotational ocean current $\mathbf{v}_c = [-5\ 5]^T$ cm/s. The parameters for the gait reference signal (11) were set to $\alpha = 7$ cm, $\omega = 120°/\text{s}, \delta = 40°$ and the scaling function to $g(i) = 1$. The gains for the control system were chosen as follows: $k_\phi = 20, k_{v_\phi} = 5, k_\theta = 0.5$. The look-ahead distance for the guidance law was chosen as $\Delta = 90$ cm and the integral gain as $\sigma = 2\ \frac{\text{cm}}{\text{s}}$.

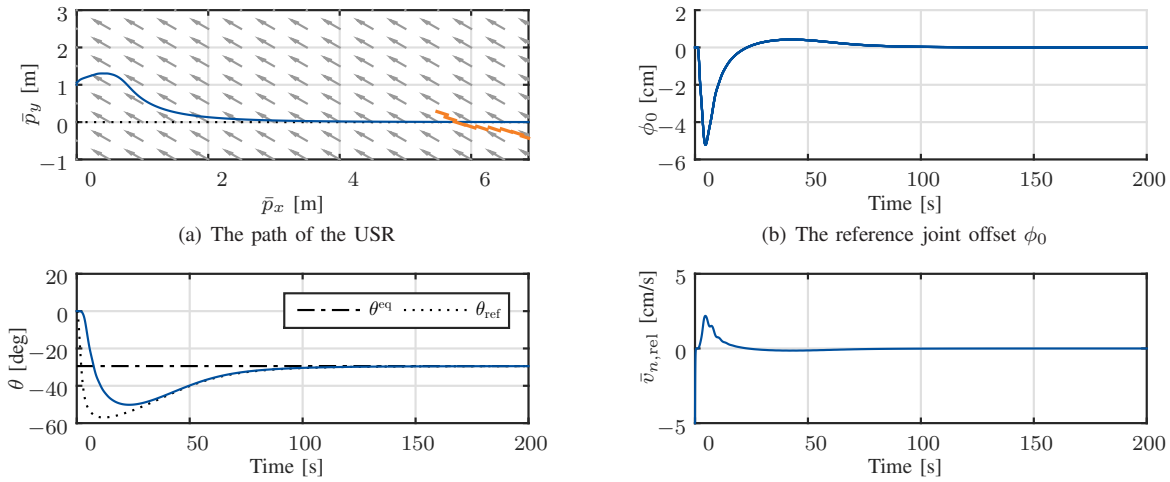

(a) The path of the USR

(b) The reference joint offset ϕ_0

(c) Heading angle

(d) Relative velocity in normal direction

Fig. 5. Simulation results: Straight line path following for an underwater snake robot with $n = 10$ links initially headed along the desired path and with an initial distance to the path of $\bar{p}_y = 1$ m

For the time derivatives of ϕ_0 and θ_{ref} that are required for the controller, third-order low-pass filter reference models were implemented. Details on these reference models can be found in Appendix C.2 in [11]. The parameters of the reference models were chosen as $\omega = \frac{\pi}{2}, \zeta = 1$.

The initial position of the robot was set to $\bar{p}_x = 0, \bar{p}_y = 1$ m, the initial orientation was $\theta = 0°$, i.e. aligned with the desired path, and the initial joint coordinates were $\boldsymbol{\phi} = 0$. All initial velocities were set to zero.

B. Simulation results

The results of the simulation are visualized in Fig. 5. The position of the USR can be seen in Fig. 5(a). After being dragged away by the ocean current in the beginning, the robot turns and converges nicely to the path. The control input ϕ_0 is visualised in Fig. 5(b). The heading angle of the robot over time can be seen in Fig. 5(c). It converges fast towards θ_{ref} provided by the ILOS guidance law, and subsequently towards the constant θ^{eq}, which was calculated from (18). Fig. 5(d) shows the relative velocity in the normal direction. It can be seen that $\bar{v}_{n,\mathrm{rel}}$ converges to zero.

VI. Conclusions and Future Work

In this paper, a control system has been introduced, which enables a USR to converge towards and follow a straight path in the presence of constant irrotational ocean currents. The control design was based on the assumption that the robot is fully submerged, neutrally buoyant, and moving with a planar sinusoidal gait. The proposed control approach applies an exponentially stabilising heading controller in order to steer the robot towards the desired heading obtained by an ILOS guidance law. Using cascaded systems theory, the system has been formally proved to be UGAS and USGES.

In future work, a velocity controller will be added, and the control system will be tested in experiments to verify the theoretical results and to investigate the performance and robustness properties. Furthermore, an extension of the control system to compensate for unknown time-varying currents and the three-dimensional case will be pursued.

Appendix

A. Function definitions

The matrix $\mathbf{A}_e(e_2)$ is defined in (24), where the notation $\bar{X}(e_2) = X + \frac{V_x\Delta - V_y(e_2+\sigma y_{\mathrm{int}}^{\mathrm{eq}})}{\sqrt{(e_2+\sigma y_{\mathrm{int}}^{\mathrm{eq}})^2+\Delta^2}}$ is used. Furthermore,

$$\mathbf{B}(e_2) = \begin{bmatrix} 0 & V_y & -\frac{\Delta \bar{X}(e_2) V_y}{(e_2+\sigma y_{\mathrm{int}}^{\mathrm{eq}})^2+\Delta^2} \end{bmatrix}^T, \tag{29}$$

$$f(e_2) = 1 - \frac{\sqrt{(\sigma y_{\mathrm{int}}^{\mathrm{eq}})^2+\Delta^2}}{\sqrt{(e_2+\sigma y_{\mathrm{int}}^{\mathrm{eq}})^2+\Delta^2}}, \tag{30}$$

and $\mathbf{H}_\xi(\boldsymbol{e}, \boldsymbol{\xi})$ is given in (25).

B. Proof of Lemma 2

The structure of the nominal system (23) is identical to the system that is presented in [15,16], where the stability of an ILOS guidance system for a surface vessel was analysed. The main difference in this paper is an additional dependence of $\bar{X}$ on e_2. Because of the similar system structure, the same Lyapunov function candidate as in [15,16] can be used.

With the quadratic Lyapunov function

$$V = \tfrac{1}{2}\sigma^2 e_1^2 + \tfrac{1}{2}e_2^2 + \tfrac{1}{2}\mu e_3^2 = \tfrac{1}{2}\boldsymbol{e}^T\mathbf{P}\boldsymbol{e}, \tag{31}$$

the notation

$$\bar{e}_i = \frac{e_i}{\sqrt{(e_2+\sigma y_{\mathrm{int}}^{\mathrm{eq}})^2+\Delta^2}}, \quad i = 1, 2, \tag{32}$$

Ass. 1, the bound $|f(e_2)| \leq \frac{|e_2|}{\sqrt{(e_2+\sigma y_{\mathrm{int}}^{\mathrm{eq}})^2+\Delta^2}}$ [15], and the easily verifiable bound $|\bar{X}(e_2)| \leq |X|+2V_{c,\max}$, the following bound on $\dot{V}$ can be found:

$$\dot{V} \leq -W_1(|\bar{e}_1|, |e_3|) - W_2(|\bar{e}_2|, |e_3|), \tag{33a}$$

$$W_1 = \sigma^3\Delta|\bar{e}_1|^2 - \mu\sigma^2\tfrac{|X|+2V_{c,\max}}{\Delta}|\bar{e}_1||e_3| + \eta\mu(|Y| - \tfrac{|X|+2V_{c,\max}}{\Delta})|e_3|^2, \tag{33b}$$

$$W_2 = \Delta \begin{bmatrix} |\bar{e}_2| & |e_3| \end{bmatrix} \begin{bmatrix} \chi_1 & -\chi_2 \\ -\chi_2 & \frac{\chi_2(2\chi_2-1)}{\chi_1} \end{bmatrix} \begin{bmatrix} |\bar{e}_2| \\ |e_3| \end{bmatrix}, \tag{33c}$$

where $0 < \eta < 1$, $\chi_1 = V_{\min} - V_{c,\max} - \sigma$, and

$$\chi_2 = (1-\eta)\chi_1\tfrac{\Delta|Y| - (|X|+2V_{c,\max})}{(|X|+2V_{c,\max})(V_{\max}+V_{c,\max}+\sigma)}. \tag{34}$$

$$\mathbf{A}_e(e_2) = \begin{bmatrix} -\frac{\sigma\Delta}{(e_2+\sigma y_{\text{int}}^{\text{eq}})^2+\Delta^2} & \frac{\Delta}{(e_2+\sigma y_{\text{int}}^{\text{eq}})^2+\Delta^2} & 0 \\ -\frac{\sigma^2\Delta}{(e_2+\sigma y_{\text{int}}^{\text{eq}})^2+\Delta^2} & \frac{\sigma\Delta}{(e_2+\sigma y_{\text{int}}^{\text{eq}})^2+\Delta^2} - \frac{v_{t,\text{rel}}}{\sqrt{(e_2+\sigma y_{\text{int}}^{\text{eq}})^2+\Delta^2}} & \frac{\Delta}{\sqrt{(e_2+\sigma y_{\text{int}}^{\text{eq}})^2+\Delta^2}} \\ \frac{\sigma^2\Delta^2\bar{X}(e_2)}{((e_2+\sigma y_{\text{int}}^{\text{eq}})^2+\Delta^2)^2} & \frac{\Delta\bar{X}(e_2)v_{t,\text{rel}}}{((e_2+\sigma y_{\text{int}}^{\text{eq}})^2+\Delta^2)^{3/2}} - \frac{\sigma\Delta^2\bar{X}(e_2)}{((e_2+\sigma y_{\text{int}}^{\text{eq}})^2+\Delta^2)^2} & Y - \frac{\Delta^2\bar{X}(e_2)}{((e_2+\sigma y_{\text{int}}^{\text{eq}})^2+\Delta^2)^{3/2}} \end{bmatrix} \tag{24}$$

$$\mathbf{H}_\xi(\boldsymbol{e},\boldsymbol{\xi}) = \begin{bmatrix} 0 & 0 \\ \frac{\gamma_1}{\theta} & 0 \\ -\frac{\Delta\bar{X}(e_2)-\Delta\gamma_2}{(e_2+\sigma y_{\text{int}}^{\text{eq}})^2+\Delta^2}\frac{\gamma_1}{\theta} - \frac{\Delta f_2(\boldsymbol{e})+\Delta V_y f(e_2)}{(e_2+\sigma y_{\text{int}}^{\text{eq}})^2+\Delta^2}\frac{\gamma_2}{\theta} & \gamma_2+\bar{X}(e_2) \end{bmatrix}, \tag{25}$$

$$\gamma_1(e_2,e_3,\widetilde{\theta}) = \sin\widetilde{\theta}\frac{\Delta v_{t,\text{rel}}+(e_2+\sigma y_{\text{int}}^{\text{eq}})e_3}{\sqrt{(e_2+\sigma y_{\text{int}}^{\text{eq}})^2+\Delta^2}} + (1-\cos\widetilde{\theta})\frac{(e_2+\sigma y_{\text{int}}^{\text{eq}})v_{t,\text{rel}}-\Delta e_3}{\sqrt{(e_2+\sigma y_{\text{int}}^{\text{eq}})^2+\Delta^2}} \tag{26}$$

$$\gamma_2(e_2,\widetilde{\theta}) = \sin\widetilde{\theta}\frac{\Delta V_y+(e_2+\sigma y_{\text{int}}^{\text{eq}})V_x}{\sqrt{(e_2+\sigma y_{\text{int}}^{\text{eq}})^2+\Delta^2}} + (1-\cos\widetilde{\theta})\frac{(e_2+\sigma y_{\text{int}}^{\text{eq}})V_y-\Delta V_x}{\sqrt{(e_2+\sigma y_{\text{int}}^{\text{eq}})^2+\Delta^2}} \tag{27}$$

$$f_2(\boldsymbol{e}) = -\frac{\sigma^2\Delta}{(e_2+\sigma y_{\text{int}}^{\text{eq}})^2+\Delta^2}e_1 + \Big(\frac{\sigma\Delta}{(e_2+\sigma y_{\text{int}}^{\text{eq}})^2+\Delta^2} - \frac{v_{t,\text{rel}}}{\sqrt{(e_2+\sigma y_{\text{int}}^{\text{eq}})^2+\Delta^2}}\Big)e_2 + \frac{\Delta}{\sqrt{(e_2+\sigma y_{\text{int}}^{\text{eq}})^2+\Delta^2}}e_3 \tag{28}$$

For (33c) and (34) to hold, μ is chosen as

$$\mu = \frac{\Delta^2(2\chi_2-1)}{(|X|+2V_{c,\max})(V_{\max}+V_{c,\max}+\sigma)}. \tag{35}$$

Following standard Lyapunov theory, the nominal system (23) is UGAS if V is positive definite and $\dot{V}$ is negative definite, which is equivalent to both W_1, W_2 being positive definite. It is straightforward to verify that the conditions

$$0 < \mu < \frac{4\eta\Delta^2(\Delta|Y|-(|X|+2V_{c,\max}))}{\sigma(|X|+2V_{c,\max})^2}, \tag{36}$$

$$\Delta > \frac{|X|+2V_{c,\max}}{|Y|} \tag{37}$$

ensure positive definiteness of V and W_1. Inequality (36) can be guaranteed with a proper choice of η, which will be defined in the next paragraph, while (37) is implied by condition (17a). In order to achieve positive definiteness of W_2, χ_1 and χ_2 have to fulfil $\chi_1 > 0$ and $\chi_2 > 1$. The latter condition also ensures that $\mu > 0$ holds. The first condition, $\chi_1 > 0$, is guaranteed by Ass. 3 and (17b), whereas the second one, $\chi_2 > 1$, is implied by (17) and the choice $\eta = \frac{1}{5}$, which also ensures that (36) holds. We can therefore conclude that both V, W_1 and W_2 are positive definite, and the equilibrium of the nominal system (23) is UGAS.

In addition, the single terms of W_1, W_2 can be assembled into a matrix, which leads to the expression

$$\dot{V} \leq -\begin{bmatrix}|\bar{e}_1|, & |\bar{e}_2|, & |e_3|\end{bmatrix}\mathbf{Q}\begin{bmatrix}|\bar{e}_1| \\ |\bar{e}_2| \\ |e_3|\end{bmatrix}, \tag{38}$$

where

$$\mathbf{Q} = \begin{bmatrix} \sigma^3\Delta & 0 & -\mu\sigma^2\frac{|X|+2V_{c,\max}}{2\Delta} \\ 0 & \Delta\chi_1 & -\Delta\chi_2 \\ -\mu\sigma^2\frac{|X|+2V_{c,\max}}{2\Delta} & -\Delta\chi_2 & \mu\frac{\Delta|Y|-|X|-2V_{c,\max}}{\Delta} \end{bmatrix} \tag{39}$$

is a time-invariant, positive definite matrix. From [31] it follows that $\dot{V}$ is bounded by

$$\dot{V} \leq -q_{\min}\begin{bmatrix}|\bar{e}_1|, & |\bar{e}_2|, & |e_3|\end{bmatrix}\begin{bmatrix}|\bar{e}_1| \\ |\bar{e}_2| \\ |e_3|\end{bmatrix}, \tag{40}$$

with $q_{\min}$ being the smallest eigenvalue of $\mathbf{Q}$. It is pointed out in [18] that UGES cannot be achieved for LOS guidance law error dynamics, because the system gain of the cross-track error e_2 decreases with the magnitude of the cross-track error. The same holds for the dynamics of the integral state e_1 [16]. By combining (32) and (40), this behaviour can also be observed in the structure of $\dot{V}$:

$$\dot{V} \leq -\frac{\lambda_{\min}}{(e_2+\sigma y_{\text{int}}^{\text{eq}})^2+\Delta^2}(|e_1|^2+|e_2|^2) - \lambda_{\min}|e_3|^2 \tag{41}$$

where the denominator leads to a slow convergence rate in e_1 and e_2 for large e_2. In order to prove that the system is still USGES, the function

$$\phi(e_2) = \min\{\lambda_{\min}, \frac{\lambda_{\min}}{(e_2+\sigma y_{\text{int}}^{\text{eq}})^2+\Delta^2}\} \tag{42}$$

is defined. It can be shown that for any ball $\mathcal{B}_r = \{|e_2| \leq r\}$,

$$\phi(e_2) \geq \min\{\lambda_{\min}, \frac{\lambda_{\min}}{(r+\kappa)^2+\Delta^2}\} = c(r), \tag{43}$$

with the bound on $|\sigma y_{\text{int}}^{\text{eq}}|$ similar to the one in [16]:

$$|\sigma y_{\text{int}}^{\text{eq}}| \leq \frac{\Delta V_{c,\max}}{\sqrt{V_{\min}^2-V_{c,\max}^2}} = \kappa. \tag{44}$$

With (43) and (41) and the UGAS property, the following expression holds on any ball $\mathcal{B}_r = \{|e_2| \leq r\}$:

$$\dot{V} \leq -c(r)\|\boldsymbol{e}\|^2. \tag{45}$$

From (31) follows that

$$\tfrac{1}{2}p_{\min}\|\boldsymbol{e}\|^2 \leq V \leq \tfrac{1}{2}p_{\max}\|\boldsymbol{e}\|^2, \tag{46}$$

where $p_{\min} = \min\{\sigma^2, 1, \mu\}$ and $p_{\max} = \max\{\sigma^2, 1, \mu\}$. With (46) and (45) , it can be seen that

$$\dot{V} \leq -2\frac{c(r)}{p_{\max}}V. \tag{47}$$

We can now invoke the comparison lemma [31], which leads to the following relation:

$$V(t,x) \leq V(t_0,x(t_0))e^{-2\frac{c(r)}{p_{\max}}(t-t_0)}. \tag{48}$$

With (46) it can be concluded that

$$\begin{aligned}\|\boldsymbol{e}(t)\| &\leq \sqrt{2\frac{V(t,x)}{p_{\min}}} \leq \sqrt{2\frac{V(t_0,x(t_0))e^{-2\frac{c(r)}{p_{\max}}(t-t_0)}}{p_{\min}}} \\ &\leq \sqrt{\frac{p_{\max}\|\boldsymbol{e}(t_0)\|^2}{p_{\min}}}e^{-\frac{c(r)}{p_{\max}}(t-t_0)} \\ &\leq \sqrt{\frac{p_{\max}}{p_{\min}}}e^{-\frac{c(r)}{p_{\max}}(t-t_0)}\|\boldsymbol{e}(t_0)\|\end{aligned} \tag{49}$$

for all $t \geq t_0$ and any $r > 0$. We can thus conclude that the equilibrium of system (23) is USGES (Def. 1). ■

C. Proof of Lemma 3

According to Appendix A in [31], the induced 2-norm of the matrix $\mathbf{H}_\xi$ satisfies

$$\begin{aligned}\|\mathbf{H}_\xi\|_2 &\leq \sqrt{2}\max_j \sum_{i=1}^{3} |\{\mathbf{H}_\xi\}_{ij}| \\ &\leq \sqrt{2}\Big(|\tfrac{\gamma_1}{\tilde{\theta}}| + |-\tfrac{\Delta\bar{X}(e_2)-\Delta\gamma_2}{(e_2+\sigma y_{\text{int}}^{\text{eq}})^2+\Delta^2}\tfrac{\gamma_1}{\tilde{\theta}}| \\ &\quad + |\tfrac{\Delta f_2(\boldsymbol{e})+\Delta V_y f(e_2)}{(e_2+\sigma y_{\text{int}}^{\text{eq}})^2+\Delta^2}\tfrac{\gamma_2}{\tilde{\theta}}| + |\gamma_2| + |\bar{X}(e_2)|\Big).\end{aligned} \tag{50}$$

The final expression

$$\|\mathbf{H}_\xi\|_2 \leq \mathcal{F}_1 + \mathcal{F}_2\|\boldsymbol{e}\|_2, \tag{51a}$$

$$\mathcal{F}_1 = \sqrt{2}\left(2V_{\max} + \tfrac{(|X|+8V_{c,\max})(\Delta+2V_{\max})}{\Delta}\right), \tag{51b}$$

$$\begin{aligned}\mathcal{F}_2 = \sqrt{2}\Big(&\tfrac{4V_{c,\max}(\sigma^2+\sigma+V_{\max}+V_{c,\max}+\Delta)}{\Delta^2} \\ &+ \tfrac{2(|X|+8V_{c,\max})}{\Delta} + 2\Big)\end{aligned} \tag{51c}$$

follows from (50) with Ass. 2, the bound on $\bar{X}(e_2)$ in App. B, and the following bounds on the single parts of $\mathbf{H}_\xi$:

$$\begin{aligned}|\tfrac{\gamma_1}{\tilde{\theta}}| &\leq 2V_{\max} + 2|e_3|, \qquad |\tfrac{\gamma_2}{\tilde{\theta}}| \leq 4V_{c,\max}, \\ |\gamma_2| &\leq 6V_{c,\max}, \qquad |f(e_2)| \leq \tfrac{|e_2|}{\Delta}, \\ |f_2(\boldsymbol{e})| &\leq \tfrac{\sigma^2}{\Delta}|e_1| + \tfrac{\sigma+V_{\max}}{\Delta}|e_2| + |e_3|.\end{aligned} \tag{52}$$

■

REFERENCES

[1] E. Kelasidi, K. Y. Pettersen, J. T. Gravdahl, and P. Liljebäck, "Modeling of underwater snake robots," in *Proc. IEEE Int. Conf. Robotics and Automation*, Hong Kong, China, May, Jun. 2014.

[2] K. Mclsaac and J. Ostrowski, "A geometric approach to anguilliform locomotion: modelling of an underwater eel robot," in *Proc. IEEE Int. Conf. Robotics and Automation*, Detroit, MI, May 1999.

[3] A. J. Wiens and M. Nahon, "Optimally efficient swimming in hyper-redundant mechanisms: control, design, and energy recovery," *Bioinspiration & Biomimetics*, vol. 7, no. 4, 2012.

[4] M. Porez, F. Boyer, and A. J. Ijspeert, "Improved lighthill fish swimming model for bio-inspired robots: Modeling, computational aspects and experimental comparisons," *Int. J. Robot. Res.*, vol. 33, no. 10, pp. 1322–1341, 2014.

[5] A. Crespi and A. J. Ijspeert, "AmphiBot II: An amphibious snake robot that crawls and swims using a central pattern generator," in *Proc. 9th Int. Conf. Climbing and Walking Robots*, Brussels, Belgium, Sep. 2006.

[6] H. Yamada, S. Chigisaki, M. Mori, K. Takita, K. Ogami, and S. Hirose, "Development of amphibious snake-like robot ACM-R5," in *Proc. 36th Int. Symp. Robotics*, Tokyo, 2005.

[7] P. Liljebäck, Ø. Stavdahl, K. Pettersen, and J. Gravdahl, "Mamba - A waterproof snake robot with tactile sensing," in *Proc. IEEE/RSJ Int. Conf. Intelligent Robots and Systems*, Chicago, IL, Sep. 2014.

[8] L. Lapierre and B. Jouvencel, "Path following control for an eel-like robot," in *Proc. Oceans 2005 - Europe*, Brest, France, Jun. 2005.

[9] J. Guo, "A waypoint-tracking controller for a biomimetic autonomous underwater vehicle," *Ocean Engineering*, vol. 33, no. 17-18, pp. 2369–2380, 2006.

[10] P. Liljebäck, I. U. Haugstuen, and K. Y. Pettersen, "Path following control of planar snake robots using a cascaded approach," *IEEE Trans. Control Syst. Technol.*, vol. 20, no. 1, pp. 111–126, 2012.

[11] P. Liljebäck, K. Y. Pettersen, Ø. Stavdahl, and J. T. Gravdahl, *Snake Robots: Modelling, Mechatronics, and Control*, ser. Advances in Industrial Control. Springer London, 2012.

[12] E. Rezapour, H. A., K. Y. Pettersen, A. Mohammadi, and M. Maggiore, "Virtual holonomic constraint based direction following control of planar snake robots described by a simplified model," in *Proc. IEEE Conf. Control Applications*, Antibes, France, Oct. 2014.

[13] E. Børhaug, A. Pavlov, and K. Y. Pettersen, "Integral LOS control for path following of underactuated marine surface vessels in the presence of constant ocean currents," in *Proc. 47th IEEE Conf. Decision and Control*, Cancun, Mexico, Dec. 2008.

[14] D. J. W. Belleter and K. Y. Pettersen, "Path following for formations of underactuated marine vessels under influence of constant ocean currents," in *Proc. 53rd IEEE Conf. Decision and Control*, Los Angeles, CA, Dec. 2014.

[15] W. Caharija, M. Candeloro, K. Y. Pettersen, and A. J. Sørensen, "Relative velocity control and integral LOS for path following of underactuated surface vessels," in *Proc. 9th IFAC Conf. Manoeuvring and Control of Marine Craft*, Arenzano, Italy, Sep. 2012.

[16] M. S. Wiig, K. Y. Pettersen, and T. R. Krogstad, "Uniform semiglobal exponential stability of integral line-of-sight guidance laws," in *Proc. 10th IFAC Conf. Manoeuvring and Control of Marine Craft*, Copenhagen, Denmark, Aug. 2015.

[17] W. Caharija, K. Y. Pettersen, J. T. Gravdahl, and E. Børhaug, "Path following of underactuated autonomous underwater vehicles in the presence of ocean currents," in *Proc. 51st IEEE Conf. Decision and Control*, Maui, HI, Dec. 2012.

[18] T. I. Fossen and K. Y. Pettersen, "On uniform semiglobal exponential stability (USGES) of proportional line-of-sight guidance laws," *Automatica*, vol. 50, no. 11, pp. 2912–2917, 2014.

[19] E. Kelasidi, K. Y. Pettersen, P. Liljebäck, and J. T. Gravdahl, "Integral line-of-sight for path following of underwater snake robots," in *Proc. IEEE Conf. Control Applications*, Antibes, France, Oct. 2014.

[20] A. M. Kohl, E. Kelasidi, K. Y. Pettersen, and J. T. Gravdahl, "A control-oriented model of underwater snake robots exposed to currents," in *Proc. IEEE Conf. Control Applications*, Sydney, Australia, Sep. 2015.

[21] A. M. Kohl, K. Y. Pettersen, E. Kelasidi, and J. T. Gravdahl, "Analysis of underwater snake robot locomotion based on a control-oriented model," in *Proc. IEEE Int. Conf. Robotics and Biomimetics*, Zhuhai, China, Dec. 2015.

[22] A. Loría and E. Panteley, "Cascaded nonlinear time-varying systems: Analysis and design," in *Advanced Topics in Control Systems Theory: Lecture Notes from FAP 2004*, F. Lamnabhi-Lagarrigue, A. Loría, and E. Panteley, Eds. Springer London Ltd., 2005, ch. 2, pp. 23–64.

[23] E. Panteley and A. Loría, "On global uniform asymptotic stability of nonlinear time-varying systems in cascade," *Systems & Control Letters*, vol. 33, no. 2, pp. 131–138, 1998.

[24] O. J. Sørdalen and O. Egeland, "Exponential stabilization of nonholonomic chained systems," *IEEE Trans. Autom. Control*, vol. 40, no. 1, pp. 35–49, 1995.

[25] E. Kelasidi, K. Y. Pettersen, and J. T. Gravdahl, "A control-oriented model of underwater snake robots," in *Proc. IEEE Int. Conf. Robotics and Biomimetics*, Bali, Indonesia, Dec. 2014.

[26] P. Liljebäck, K. Y. Pettersen, Ø. Stavdahl, and J. T. Gravdahl, "A simplified model of planar snake robot locomotion," in *Proc. IEEE/RSJ Int. Conf. Intelligent Robots and Systems*, Taipei, Taiwan, Oct. 2010.

[27] E. Kelasidi, P. Liljebäck, K. Y. Pettersen, and J. T. Gravdahl, "Experimental investigation of efficient locomotion of underwater snake robots for lateral undulation and eel-like motion patterns," *Robotics and Biomimetics*, vol. 2, no. 1, 2015.

[28] K. Do and J. Pan, "Global tracking control of underactuated ships with off-diagonal terms," in *Proc. 42nd IEEE Conf. Decision and Control*, Maui, HI, Dec. 2003.

[29] E. Fredriksen and K. Y. Pettersen, "Global κ-exponential way-point manouvring of ships: Theory and Experiments," *Automatica*, vol. 42, no. 4, pp. 677–687, 2006.

[30] T. I. Fossen, *Handbook of Marine Craft Hydrodynamics and Motion Control*. Wiley, 2011.

[31] H. Khalil, *Nonlinear Systems*, 3rd ed. Prentice Hall, 2002.

[32] E. Kelasidi, P. Liljebäck, K. Y. Pettersen, and J. T. Gravdahl, "Biologically inspired swimming snake robots: Modeling, control and experimental investigation," accepted. *IEEE Robotics and Automation Magazine* 2015.